Review of Geological Controls on Resistivity in Uplifted Basins: Insights from the Norwegian Barents Shelf*

Kim Senger[1,3], Thomas Birchall[2,3], Sverre Ohm[2,4], Snorre Olaussen[2,3], Kei Ogata[5]

Search and Discovery Article #30535 (2017)**
Posted December 18, 2017

*Adapted from extended abstract prepared in conjunction with oral presentation given at AAPG/SEG 2017 International Conference and Exhibition, London, England, October 15-18, 2017

[1]Department of Arctic Geology, University Centre in Svalbard, Longyearbyen, Norway (kims@unis.no)
[2]Department of Arctic Geology, University Centre in Svalbard, Longyearbyen, Norway
[3]Research Centre for Arctic Petroleum Exploration – ARCEx
[4]Institute for Petroleum Technology, University of Stavanger, Stavanger, Norway
[5]Department of Earth Science, Vrije Universiteit, Amsterdam, Netherlands

Abstract

Resistivity is mainly controlled by the presence of electrically conductive fluids, i.e. brine, capable of transmitting an electric current through the investigated geological formation. In sedimentary basins, where conductive matrix minerals are rare, resistivity is primarily controlled by: 1) porosity, 2) brine conductivity, 3) connectivity of pore space, and 4) brine saturation. In recent years, the use of controlled-source electromagnetic (CSEM) data allows for pre-drill resistivity mapping at both prospect and regional scale. However, interpretation of CSEM data relies heavily on understanding and quantifying the geological parameters that influence resistivity. In this contribution, we present a review of the geological parameters controlling resistivity variation, presenting case studies from > 100 released exploration boreholes from the Barents shelf. The highest resistivity (> 10 000 Ωm) is evident in the relatively shallow, highly porous and hydrocarbon-bearing sandstones of the Upper Triassic-Middle Jurassic Realgrunnen Subgroup, which are reported from 37 boreholes. Pay zone resistivity is primarily controlled by reservoir quality (i.e. porosity and V_{shale}) and fluid phase (i.e. gas vs oil and water saturation). The Realgrunnen Subgroup reservoir is, in places, capped by Upper Jurassic organic rich shales of the Hekkingen Formation. In the investigated wells, these shales exhibit enhanced resistivity compared to the background, though rarely exceeding 20 Ωm and never exceeding 55 Ωm. Marine mudstones often show good correlation between measured organic richness and the resistivity/sonic velocity log signatures. In contrast to normally compacted basins, where vertical resistivity variations in the shallow subsurface are controlled by the effects of temperature and salinity, resistivity variations in the exhumed Barents shelf are related to effects of porosity reduction due to extensive mechanical and chemical compaction. We conclude that the present-day resistivity distribution on the Barents shelf is affected by diagenesis, fluid distribution, and total organic carbon of shales.

Introduction

Exploration for hydrocarbons is challenging, particularly so in frontier sedimentary basins where limited data are available. The Barents Sea is

such an example, estimated to contain 48% of Norwegian undiscovered resources, corresponding to approximately 1.4 billion Sm^3 of oil equivalents (NPD, 2015). The area open to petroleum exploration in the Norwegian segment of the Barents Sea covers almost 300 000 km^2, where 133 wells (i.e. one well per 2200 km^2) were drilled since the first exploration well, 7119/12-1, in 1980. Recent exploration success, including the 7324/8-1 Wisting oil discovery (38.3 mill Sm^3; 241 MMboe; NPD, 2016), can be partly attributed to the integrated use of marine controlled source electro-magnetic (CSEM) data. CSEM was developed in the early 2000s in order to remotely detect thin resistors prior to drilling (Constable and Weiss, 2006: Eidesmo et al., 2002). As with any exploration technique, CSEM has its limitations that interpreters must be aware of potential pitfalls. One of the key aspects to consider with CSEM is sensitivity to a given target, governed by the target size (i.e. area), target transverse resistance (i.e. resistivity *x* thickness), target burial depth, the background resistivity and its complexity (MacGregor, 2012). The obvious benefit of using CSEM prior to drilling is to quantify the subsurface resistivity distribution, with implications for de-risking prospects (Buland et al., 2011; Fanavoll et al., 2014), pre-drill hydrocarbon saturation prediction (Løseth et al., 2014), delineating discoveries and constraining resource estimates (Baltar and Barker, 2015).

Resistivity is derived from non-seismic exploration methods and thus represents an independent geophysical measurement of the same subsurface. This fact may be used to update the velocity model used during seismic processing ((Panzner et al., 2016) or to construct start models for CSEM inversion using seismic velocities (e.g., Werthmüller et al., 2013). Nonetheless, such multi-physical workflows require robust and site-specific cross-property relationships between electric (i.e. resistivity) and non-electric (e.g., seismic velocity) parameters. Porosity is typically used (e.g., Carcione et al., 2007), but caution must be taken as resistivity is much more sensitive to fluid effects that include salinity, temperature, pressure, and saturation. Resistivity has been measured in wireline logging since 1928 (Schlumberger et al., 1934). Archie (1942) proposed an empirical law relating resistivity to fluid saturation. Worthington 1993 provides an overview of some of the countless publications that followed, and highlight the challenges associated particularly with the shale effect on pay zone resistivity (e.g., Simandoux, 1963; Worthington, 1982). The focus was on the reservoir intervals, with some notable exceptions where resistivity logs were actively used in non-reservoir sections. MacGregor (1965) and Zhang (2011), for instance, outline methods to quantify the top of overpressured zones. Passey et al. (1990) integrate the resistivity and sonic logs to quantify the organic richness of source rocks.

Quantitative links between resistivity, measured either at well or CSEM scale, and its underlying geological drivers are still remarkably poorly documented. These include both the background trends, but also resistivity variation in the pay zone and the organic-rich source rock. In this contribution, we present a regional study of the Barents shelf, relying on well data to illustrate the overall resistivity variation in this uplifted sedimentary basin system. We focus on four objectives: 1) Provide a regional overview of vertical resistivity variation across the Barents shelf, 2) Illustrate resistivity variation in the hydrocarbon-bearing sandstone reservoirs of the Middle Jurassic Realgrunnen Subgroup, 3) Illustrate resistivity variation in the organic-rich source rock of the Late Jurassic Hekkingen Formation, and 4) Discuss these units in terms of geological controls on resistivity variation.

Beyond Archie: What Is Resistivity Controlled By?

Formation resistivity, the inverse of conductivity, is primarily controlled by the presence of electrically conductive fluids (i.e. brine) that transmit an electric current through the formation (Figure 1). In sedimentary basins where the matrix generally comprises insulating material, it is largely controlled by four factors: 1) porosity, 2) brine conductivity, 3) pore space connectivity, and 4) brine saturation. Porosity determines

how much conductive brine is available, brine conductivity, a function of temperature and salinity, determines how easily the current will be transported, connectivity describes how easily the current can flow across the target (i.e. permeability) and saturation determines whether some of the conductive brine has been mixed/replaced by a non-conductive fluid such as hydrocarbons. While these factors are qualitatively reasonably well known, there is a clear need for quantifying the significance of any individual parameter influencing the overall formation resistivity. In exploration wells, many of the key parameters (e.g., porosity, temperature, brine salinity) can be derived from non-electrical logs and fluid samples. Away from wells, where resistivity is derived from CSEM data, universal rock physical relationships must be applied, integrating non-electrical data (e.g., seismic velocity) where possible, in a joint interpretation workflow (Senger et al., 2015).

Resistivity is measured at a range of scales, directions and frequencies, and robust upscaling and downscaling methods are required to relate CSEM-derived resistivity to well-logged resistivity. Baltar and Roth (2013) introduced the concept of anomalous transverse resistance (ATR), a thickness-resistivity product that describes the cumulative resistivity contrast in hydrocarbon-bearing reservoirs. ATR can thus be used to accurately predict true pay zone resistivity from CSEM data, provided that the reservoir thickness is known or assumed to be known, and is therefore a critical component of pre-drill volumetric assessments (e.g., Baltar and Barker, 2015). In the context of stacked reservoirs, or hydrocarbon-bearing sandstones overlain by resistive organic-rich shales, the ATR equivalence principle can be applied to quantify the relative contribution of the two resistors. In addition, resistivity is a highly anisotropic and scale-dependent parameter, with electrical conduction varying significantly with the direction and scale of the measurement, ranging from plug-scale in the lab (North et al., 2013), to well-scale (Ellis et al., 2010) to CSEM-scale (Løseth et al., 2014). Modern 3D CSEM inversion is anisotropic (i.e. one derives both the vertical, R_v, and horizontal, R_h, resistivity; anisotropy = R_v/R_h), while most vertical exploration boreholes are primarily sensitive to horizontal resistivity. Boreholes equipped with tri-axial resistivity tools able to derive the vertical resistivity are rare (e.g., Clavaud, 2008), particularly in the non-reservoir sections, but the 7220/8-1 Skrugard well in the Barents Sea is a notable exception (Løseth et al., 2014). The scale of measurement also controls anisotropy, and anisotropy at well scale cannot be compared to anisotropy at CSEM scale.

Geological Setting and Exploration History

In this contribution we focus on the Norwegian part of the Barents Sea, the western Barents shelf, where hydrocarbon exploration commenced onshore Svalbard in the 1960s (Nøttvedt et al., 1993) and offshore in the Hammerfest Basin in the 1980s (Henriksen et al., 2011b). The geological history of the Barents shelf is discussed at length in numerous publications (e.g., Faleide et al., 2008; Faleide et al., 1993; Grogan et al., 1999; Henriksen et al., 2011b; Worsley, 2008 and references therein) and is only briefly reviewed here. Three major tectonic phases are identified in the greater Barents Sea by Henriksen et al. (2011b), starting with the Paleozoic Caledonian Orogeny in the west that resulted in a broadly easterly sediment distribution, comprising carbonate platform deposits which host the recent Gohta and Alta oil discoveries (e.g., Rønnevik, 2015). The Late Paleozoic-Mesozoic Uralide Orogeny in the east led to the uplift of Novaya Zemlya, clastic deposition and a shift in the sedimentation direction towards the north-west. This large-scale shelf edge progradation is readily identified as clinoforms in the Triassic section of the Barents shelf on seismic data (e.g., Glørstad-Clark et al., 2010; Høy and Lundschien, 2011), prograding as far as Svalbard by the Carnian (Anell et al., 2014). The Goliat oil field is partly producing from Middle Triassic sandstone reservoirs of the Kobbe Formation (Duran et al., 2013; Mulrooney et al., 2017). Late Mesozoic-Cenozoic rifting related to the final opening of the North Atlantic and crustal break-up, resulted in the current basin configuration and the formation of, amongst others, the Hammerfest Basin. The Snøhvit Field is producing gas from Late Triassic-Middle Jurassic sandstones of the Realgrunnen Subgroup (e.g., Wennberg et al., 2008), and many recent discoveries

including Norvarg, Johan Castberg, and Wisting all host hydrocarbons in this interval. Significant uplift and net erosion occurred in at least three phases in the Cenozoic (Henriksen et al., 2011a), culminating with enhanced glacial erosion during the Neogene. Net erosion varies from 0 to 3000 m (Figure 2A), with uplift impacting on reservoir quality (i.e. diagenesis), trapping integrity (e.g., decompaction fracturing), source rock maturity (Ohm et al., 2008) and fluid (re-)distribution. Due to the laterally varying uplift, the sedimentary units targeted for petroleum in the south-western Barents shelf are presently exposed onshore on the Svalbard archipelago. Representative burial history curves are illustrated in Figure 2C.

Methods and Data

For this study we use data from both offshore released exploration wells from the Barents Sea and onshore wells from Svalbard. NPD's interactive FactMaps were used to filter offshore wells where hydrocarbons were reported in the Realgrunnen Subgroup, representing over 30% of all exploration wells drilled in the Barents shelf. Wells with no hydrocarbons in the Realgrunnen Subgroup were utilized to quantify background resistivity variation. Composite logs from NPD (2016) were used in the evaluation with formation tops and fluid contact depths.

Results

We present our results by investigating large-scale resistivity-depth trends for selected wells before specifically addressing resistivity variation in organic-rich shales and reservoir sandstones.

Vertical Background Resistivity Trends

Figure 3 illustrates resistivity variation with depth in four wells covering the majority of the Phanerozoic stratigraphy. On a kilometer scale and in the absence of hydrocarbons, vertical trends are dominated by porosity effects, often showing compaction-driven trends as exemplified in wells 7229/11-1 and 7225/3-1. As shale is buried, porosity decreases with depth in a normal compaction trend (Clavaud, 2008; Mouchet and Mitchell, 1989). Overpressured zones display anomalously high porosities at a given depth and, since it is impossible to take direct pressure measurements in low permeability shale-dominated intervals, resistivity logs can be used to identify these zones (e.g., MacGregor, 1965; Zhang, 2011). The method is most effective when rocks are at their maximum burial depth, and thus is most applicable in the western margin of the Barents Sea, which has not undergone extensive exhumation. Wells 7229/11-1 and 7225/3-1 are both normally pressured and show increasing resistivity with depth typical of normal compaction (Figure 3). In well 7219/8-1 S, overpressured to approximately 220 bar in the reservoir section at 4525 m (Figure 3; NPD, 2016), a reversal of resistivity at 2600 m may mark the onset of overpressure. Well 7119/9-1 suffered a kick at 2744 m, resistivity reverses approximately 300 m above top reservoir likely representing the onset of overpressure.

Organic Rich Shale Versus Reservoir Sandstones

Figure 4 illustrates the resistivity measured in three significant hydrocarbon discoveries. All three wells share the same exploration play, the shallow marine and fluviodeltaic sandstones of the Late Triassic to Middle Jurassic Realgrunnen Subgroup (Halland et al., 2013). The reservoir is sealed by Late Jurassic shales, including the organic-rich Hekkingen Formation source rock interval. The high resistivity, well above 1000

Ωm, in the pay-bearing sections sharply contrasts with the lowest resistivity measured in these wells in the high-porosity, brine-bearing sandstones in the lower part of the Realgrunnen Subgroup reservoir. Interestingly, the pay zone resistivity is lower in the gas zone than in the oil zone in the 7220/8-1 well, which is attributed to lower hydrocarbon saturation due to poorer reservoir quality in the upper part (Figure 4B). To quantify resistivity variation in the 37 hydrocarbon-bearing wells in the database, a discrete log was constructed to differentiate electric facies (Figure 4A). This includes two overburden zones, with the "glacial overburden" often not logged or with anomalously large resistivity values that may represent fresh pore water or measurement errors. The main "overburden" zone comprises the Paleogene and Cretaceous formations, the base of which is defined by the Top Hekkingen Formation. The zone quantifies the background resistivity as well as the depth to the reservoir. The Fuglen Formation is typically sandwiched between the Hekkingen Formation and the Realgrunnen Subgroup, and forms the zone "Top Reservoir-Base Hekkingen". The Realgrunnen Subgroup is itself divided based on the fluid contacts reported by NPD (2016), into the gas, oil, and water-bearing zones. Penetrated strata deeper than the zone of interest are collectively referred to as "underburden".

The same electro-facies classification has been used to illustrate the variability in resistivity in selected discovery wells spanning the entire Barents Sea (Figure 5). The overburden typically varies between 2 and 3 Ωm, and is higher in the northern wells 7324/8-1 (3-5 Ωm) and 7225/3-1 (4 Ωm), as well as the south-western well 7019/1-1 (7 Ωm). Onshore Svalbard, background resistivity is highest, averaging ca 57 Ωm in the Mesozoic section. Resistivity in the overburden never exceeds 10 Ωm within the upper quartile, but higher values are often associated with the relatively thin glacial overburden directly beneath the seafloor surface (Figure 4). The Hekkingen Formation is present in 34 of the 37 discovery wells investigated, and ranges from 9 m (7219/8-2) to 196 m (7120/12-3) in thickness, with an average of 70 m. It displays considerable variability in measured resistivity, presumably related to the level of maturity and organic richness. In most wells the resistivity is entirely below 10 Ωm. In wells 7220/5-1, 7124/3-1, and 7125/4-1 there is virtually no contrast in the resistivity in the Hekkingen Formation compared to the overburden zone. In wells 7324/8-1 and 7219/8-2 there is some overlap between the overburden and Hekkingen Formation resistivity. In the remaining wells, resistivity is significantly higher in the Hekkingen Formation compared to the overburden, but it never exceeds 100 Ωm in the upper quartile. The highest recorded resistivity in the Hekkingen Formation in any of the Barents Sea wells is approximately 55 Ωm in well 7121/9-1. Clearly, there is a bias given that the vast majority of exploration wells are drilled on structures and not in basins where source rock intervals are likely to be thicker and more resistive due to active hydrocarbon generation. The resistivity range (upper to lower quartile) typically varies between 7 and 50 Ωm, and is highest in the wells within the Hammerfest Basin, for instance 7121/7-2, 7121/4-1, and 7121/5-2.

The hydrocarbon bearing zones, subdivided into gas and oil zones based on the reported fluid contacts, show the largest variation in resistivity spanning several orders of magnitude. This is thought to be controlled primarily by reservoir quality and water saturation. The lowest values are recorded in wells 7124/3-1 and 7125/4-1 south-west of the Nordkapp Basin, where pay zone resistivity is typically less than 10 Ωm. Notably, both these wells represent discoveries unlikely to be developed (NPD, 2016). Many wells exhibit pay zone resistivity ranging between 20 and 200 Ωm, however, some wells (e.g., 7324/8-1, 7220/8-1, 7220/7-1) show extremely high pay zone resistivity peaking at over 2000 Ωm. In wells where both a gas and oil zones are reported, two groups can be identified. In Group 1 (7220/7-1, 7121/4-1, 7121/5-2, 7124/3-1) the oil zone exhibits lower resistivity values, which is expected considering capillary force effects. In Group 2 (7220/5-1, 7220/8-1), however, the oil zone displays considerably higher resistivity compared to the gas zone.

Discussion

Resistivity Controls in Background

Faust (1953) proposed to aid lithological characterization by linking Archie's law (Archie, 1942) with porosity-depth trends derived partly from sonic and resistivity logs with an empirical approach. This pioneering work forms the foundation for more recent work, notably by Dræge (2010), to devise rock physics depth trends incorporating electrical resistivity. The challenge, however, is that resistivity is not solely related to porosity changes but is also affected by other factors such as temperature or salinity variation. This is well illustrated by Dell'Aversana et al. (2011) who devise a porosity-resistivity correlation but struggle to model the wide range in resistivity present for the same porosity value.

On the Barents shelf, resistivity variation in the background can be appreciated when plotting resistivity in the non-hydrocarbon bearing overburden and underburden sections in all investigated wells as a function of sonic velocity, gamma ray and depth (Figure 6). Even though this comparison involves numerous wells from the entire Barents shelf there is a clear correlation between resistivity and sonic velocity – i.e. a porosity-driven compaction trend (Figure 6C). The trend is well defined at very high sonic velocities in the Polarrev Formation but is increasingly broader at moderate sonic velocities, suggesting non-porosity effects such as temperature or salinity variation. Diagenetic effects, with lateral variation controlled by factors such as differential subsidence and uplift histories, will also contribute to the heterogeneity. Lithological effects are also apparent when comparing resistivity with gamma ray (GR; Figure 6B), where the highest GR values are recorded in organic rich shales of the Fuglen, Hekkingen and Kobbe formations. Progressively higher and lower resistivity is recorded in low GR rocks in tight Permian carbonates and clean sandstones of the Realgrunnen Subgroup, respectively.

Resistivity Controls in Organic Rich-Shales

Figure 7 illustrates resistivity variation in the organic-rich shales of the Hekkingen Formation source rock. Koevoets et al. (in review), following the method outlined by Passey et al. (1990), demonstrate a clear correlation between the sonic-resistivity overlay (i.e. Δ log R) from wireline data with Rock-Eval derived TOC values from core material in an onshore well on Svalbard (DH4, Figure 7B). There is a clear trend of increasing resistivity in areas where the Hekkingen Formation is mature, with the Hammerfest Basin wells in particular illustrating enhanced Hekkingen Formation resistivity compared to wells on the Bjarmeland platform (Figure 7B). TOC data from Rock-Eval on selected wells indicate a very convincing trend towards low velocity, high resistivity, high gamma ray, and high TOC source rock populations (Figure 7C). Work is ongoing on further quantifying the impact of shale properties on the resistivity and link this to observations from EM data in basinal areas.

Resistivity Controls in Reservoir Sandstones

Several orders of magnitude variations are apparent in resistivity within the pay bearing zones (Figure 8). In "commercial" discoveries the resistivity typically exceeds several hundred Ωm (Figure 8A). Smaller discoveries reported as "unlikely to be developed" by NPD (2016) and water-bearing wells often show high conductivity in the reservoir sandstones due to the presence of conductive brine in high quality reservoir

sandstones (Figure 8B). The primary control on resistivity is thus water saturation, with reservoir properties (i.e. porosity, V_{shale}) contributing to internal variation.

Conclusions

In this contribution, we have investigated the resistivity variation as measured in exploration boreholes in the Barents shelf. Both vertical and lateral trends are apparent, controlled by a multitude of geological factors. The following main conclusions can be drawn from this study:

- The Barents shelf has experienced significant uplift in the Cenozoic. This has affected diagenetic processes, and particularly the porosity-depth trend. This regional trend is seen at both well and basin-scale.
- Brine conductivity variation due to temperature and salinity changes likely influence resistivity in the overburden, though not to the same extent as expected in normally compacted basins such as the North Sea.
- Overpressure is present in the rapidly subsiding part of the western Barents Sea, and its onset is potentially identified on resistivity logs.
- Resistivity in organic rich shales, and in particular the Late Jurassic Hekkingen Formation source rock, is a function of both the total organic content and its maturation stage. In the investigated wells, resistivity in the Hekkingen Formation does not exceed 55 Ωm.
- The hydrocarbon bearing Realgrunnen Subgroup sandstones exhibit extremely high resistivity in excess of several hundred to thousands Ωm. This is especially valid in the significant fields and discoveries considered as commercial. In smaller discoveries where development is considered unlikely (i.e. sub-commercial), the pay zone resistivity is often less than 100 Ωm.
- We have particularly focused on parameters relevant for exploration away from well control where factors such as a resistor's transverse resistance (i.e., thickness * resistivity), its sub-seafloor depth and vertical separation to other resistors are all important when interpreting controlled-source electromagnetic data. As such, this study forms a good framework for interpreting resistivity data away from wells, such as CSEM or MT data sets. The concept of anomalous transverse resistance can be used to predict pay zone resistivity from EM data if the reservoir thickness is known or assumed.

Acknowledgements

We sincerely appreciate the generous data access, particularly from the Norwegian Petroleum Directorate through the DISKOS database and the UNIS CO_2 lab (http://co2-ccs.unis.no) for access to the CO_2 boreholes onshore Svalbard. KS acknowledges past colleagues at EMGS and its clients for many fruitful technical discussions on interpreting resistivity data. UNIS acknowledges the academic licenses of Petrel, the Blueback Toolbox and RokDoc provided by Schlumberger, Cegal, and Ikon Science, respectively. This research is jointly funded by ARCEx partners and the Research Council of Norway (grant number 228107) and the Fajutri project sponsored by ConocoPhillips and Lundin Norway.

References Cited

Anell, I., A. Braathen, and S. Olaussen, 2014, The Triassic-Early Jurassic of the Northern Barents Shelf: A Regional Understanding of the Longyearbyen CO_2 Reservoir: Norwegian Journal of Geology, v. 94/2-3, p. 83-98.

Archie, G.E., 1942, The Electrical Resistivity Log as an Aid in Determining Some Reservoir Characteristics: Petroleum Technology, v. 1422, p. 54-62.

Baltar, D., and N.D. Barker, 2015, Prospectivity Evaluation with 3D CSEM: First Break, v. 33/9, p. 55-62.

Baltar, D., and F. Roth, 2013, Reserves Estimation Methods for Prospect Evaluation with 3D CSEM Data: First Break, v. 31, p. 103-111.

Bruce, B., and G. Bowers, 2002, Pore Pressure Terminology: The Leading Edge, v. 21/2, p. 170-173.

Buland, A., L.O. Løseth, A. Becht, M. Roudot, and T. Røsten, 2011, The Value of CSEM Data in Exploration: First Break, v. 29/4, p. 69-76.

Carcione, J., B. Ursin, and J. Nordskag, 2007, Cross-Property Relations Between Electrical Conductivity and the Seismic Velocity of Rocks: Geophysics, v. 72/5, p. E193-E204.

Cavanagh, A.J., R. Di Primio, M. Scheck-Wenderoth, and B. Horsfield, 2006, Severity and Timing of Cenozoic Exhumation in the Southwestern Barents Sea: Journal of the Geological Society, v. 163/5, p. 761-774.

Clavaud, J.-B., 2008, Intrinsic Electrical Anisotropy of Shale: The Effect of Compaction: Petrophysics, v. 49/03.

Constable, S., and C.J. Weiss, 2006, Mapping Thin Resistors and Hydrocarbons with Marine EM Methods: Insights from 1D Modeling: Geophysics, v. 71/2, p. G43-G51.

Dell'Aversana, P., G. Bernasconi, F. Miotti, and D. Rovetta, 2011, Joint Inversion of Rock Properties from Sonic, Resistivity and Density Well-Log Measurements: Geophysical Prospecting, v. 59, p. 1144-1154.

Dræge, A., 2010, Rock Physics and Resistivity Depth Trends – An Integrated Approach: SEG Annual Meeting, 17-22 Oct 2010, Denver, Colorado.

Duran, E.R., R. di Primio, Z. Anka, D. Stoddart, and B. Horsfield, 2013, 3D-Basin Modelling of the Hammerfest Basin (Southwestern Barents Sea): A Quantitative Assessment of Petroleum Generation, Migration and Leakage: Marine and Petroleum Geology, v. 45, p. 281-303.

Eidesmo, T., S. Ellingsrud, L.M. MacGregor, S. Constable, M.C. Sinha, S. Johansen, F.N. Kong, and H. Westerdahl, 2002, Sea Bed Logging (SBL), A New Method for Remote and Direct Identification of Hydrocarbon Filled Layers in Deepwater Areas: First Break, v. 20, p. 144-152.

Ellis, M., M. Sinha, and R. Parr, 2010, Role of Fine-Scale Layering and Grain Alignment in the Electrical Anisotropy of Marine Sediments: First Break, v. 28/9, p. 49-57.

Faleide, J.I., F. Tsikalas, A.J. Breivik, R. Mjelde, O. Ritzmann, Ø. Engen, J. Wilson, and O. Eldholm, 2008, Structure and Evolution of the Continental Margin Off Norway and the Barents Sea: Episodes, v. 31/1, p. 82-91.

Faleide, J.I., E. Vågnes, and S.T. Gudlaugsson, 1993, Late Mesozoic-Cenozoic Evolution of the South-Western Barents Sea in a Regional Rift-Shear Tectonic Setting: Marine and Petroleum Geology, v. 10/3, v. 186-214.

Fanavoll, S., P. Gabrielsen, and S. Ellingsrud, 2014, CSEM as a Tool for Better Exploration Decisions: Case Studies from the Barents Sea, Norwegian Continental Shelf: Interpretation, v. 2/3, p. SH55-SH66.

Faust, L., 1953, A Velocity Function Including Lithologic Variation: Geophysics, v. 18/2, p. 271-288.

Glørstad-Clark, E., J.I. Faleide, B.A. Lundschien, and J.P. Nystuen, 2010, Triassic Seismic Sequence Stratigraphy and Paleogeography of the Western Barents Sea Area: Marine and Petroleum Geology, v. 27/7, p. 1448-1475.

Grogan, P., A.M. Østvedt-Ghazi, G.B. Larssen, B. Fotland, K. Nyberg, S. Dahlgren, and T. Eidvin, 1999, Structural Elements and Petroleum Geology of the Norwegian Sector of the Northern Barents Sea: Geological Society, London, Petroleum Geology Conference Series 5, p. 247-259.

Halland, E.K., J. Mujezinović, and F. Riis, 2013, CO_2 Storage Atlas Barents Sea: Norwegian Petroleum Directorate.

Henriksen, E., H.M. Bjørnseth, T.K. Hals, T. Heide, T. Kiryukhina, O.S. Kløvjan, G.B. Larssen, A.E. Ryseth, K. Rønning, K. Sollid, and A. Stoupakova, 2011a, Chapter 17 Uplift and Erosion of the Greater Barents Sea: Impact on Prospectivity and Petroleum Systems, *in* A.M. Spencer, A.F. Embry, D.L. Gautier, A.V. Stoupakova, and K. Sørensen (eds.), Arctic Petroleum Geology: Geological Society, Memoir #35, London, p. 271-281.

Henriksen, E., A.E. Ryseth, G.B. Larssen, T. Heide, K. Rønning, K. Sollid, and A.V. Stoupakova, 2011b, Chapter 10 Tectonostratigraphy of the Greater Barents Sea: Implications for Petroleum Systems, *in* A.M. Spencer, A.F. Embry, D.L. Gautier, A.V. Stoupakova, and K. Sørensen (eds.), Arctic Petroleum Geology: Geological Society, Memoir #35, London, p. 163-195.

Høy, T. and B.A. Lundschien, 2011, Chapter 15 Triassic Deltaic Sequences in the Northern Barents Sea, *in* A.M. Spencer, A.F. Embry, D.L. Gautier, A.V. Stoupakova, and K. Sørensen (eds.), Arctic Petroleum Geology: Geological Society, Memoir #35, London, p. 249-260.

Koevoets, M.J., Ø. Hammer, S. Olaussen, K. Senger, and M Smelror, in review, Facies, Bio- and Sequence Stratigraphy of the Middle Jurassic to Lower Cretaceous Agardhfjellet Formation in central Spitsbergen: Norwegian Journal of Geology.

Løseth, L.O., T. Wiik, P.A. Olsen, and J.O. Hansen, 2014, Detecting Skrugard by CSEM - Prewell Prediction and Postwell Evaluation: Interpretation, p. SH67-SH78.

MacGregor, J.R., 1965, Quantitative Determination of Reservoir Pressures from Conductivity Log: American Association of Petroleum Geologists Bulletin, v. 49, p. 1502-1511.

MacGregor, L., 2012, Integrating Seismic, CSEM, and Well-Log Data for Reservoir Characterization: The Leading Edge, v. 3, p. 268-277.

Mouchet, J.-P., and A. Mitchell, 1989, Abnormal Pressures While Drilling: Origins, Prediction, Detection, Evaluation, 2nd Edition, Technip, 255 p.

Mulrooney, M.J., J. Leutscher, and A. Braathen, 2017, A 3D Structural Analysis of the Goliat Field, Barents Sea, Norway: Marine and Petroleum Geology, v. 86: p. 192-212.

North, L., A.I. Best, J. Sothcott, and L. MacGregor, 2013, Laboratory Determination of the Full Electrical Resistivity Tensor of Heterogeneous Carbonate Rocks at Elevated Pressures: Geophysical Prospecting, v. 61/2, p. 458-470.

NPD, 2015, Resource Accounts for the Norwegian Continental Shelf as of 31 December 2015. http://www.npd.no/en/Topics/Resource-accounts-and--analysis/Temaartikler/Resource-accounts/2015/. Website accessed December 2017.

NPD, 2016. FactPages.

Nøttvedt, A., F. Livbjerg, P.S. Midbøe, and E. Rasmussen, 1993, Hydrocarbon Potential of the Central Spitsbergen Basin, *in* T.O. Vorren, E. Bergsager, Ø.A. Dahl-Stamnes, E. Holter, B. Johansen, E. Lie, and T.B. Lund (eds.), Arctic Geology and Petroleum Potential: Elsevier, Amsterdam, p. 333-361.

Ohm, S.E., D.A. Karlsen, and T.J.F. Austin, 2008, Geochemically Driven Exploration Models in Uplifted Areas: Examples from the Norwegian Barents Sea: American Association of Petroleum Geologists Bulletin, v. 92/9, p. 1191-1223.

Panzner, M., J.P. Morten, W.W. Weibull, and B. Arntsen, 2016, Integrated Seismic and Electromagnetic Model Building Applied to Improve Subbasalt Depth Imaging in the Faroe-Shetland Basin: Geophysics, v. 81/1, p. E57-E68.

Passey, Q., S. Creaney, J. Kulla, F. Moretti, and J. Stroud, 1990, A Practical Model for Organic Richness from Porosity and Resistivity Logs: American Association of Petroleum Geologists Bulletin, v. 74/12, p. 1777-1794.

Rønnevik, H.C., 2015, Exploration Strategy, Petroleum Geoscience: Springer, p. 639-651.

Schlumberger, C., M. Schlumberger, and E.G. Leonardon, 1934, Electrical Coring; A Method of Determining Bottom-Hole Data by Electrical Measurements: Transactions of the AIME, v. 110/01, p. 237-272.

Senger, K., S. Fanavoll, E. Nerland, P. Gabrielsen, R. Svendsen, B. Kjølhamar, and D. Baltar, 2015, Joint Interpretation of Electric and Elastic Measurements in Frontier Exploration: Third EAGE Workshop on Rock Physics.

Simandoux, 1963, Mesures dielectriques en milieu poreux: application a la mesure des saturations en eau: etude du comportement des massifs argileux: Revue de I'Institut Franqais du Petrole, v. 18, p. 193-215.

Wennberg, O.P., O. Malm, T. Needham, E. Edwards, S. Ottesen, F. Karlsen, L. Rennan, and R. Knipe, 2008, On the Occurrence and Formation of Open Fractures in the Jurassic Reservoir Sandstones of the Snøhvit Field, SW Barents Sea: Petroleum Geoscience, v. 14, p. 139-150.

Werthmüller, D., A. Ziolkowski, and D. Wright, 2013, Background Resistivity Model from Seismic Velocities: Geophysics, v. 78/4, p. E213-E223.

Worsley, D., 2008, The Post-Caledonian Development of Svalbard and the Western Barents Sea: Polar Research, v. 27, p. 298-317.

Worthington, P.F., 1982, The Influence of Shale Effects Upon the Electrical Resistivity of Reservoir Rocks: Geophysical Prospecting, v. 30/5, p. 673-687.

Worthington, P.F., 1993, The Uses and Abuses of the Archie Equations, 1: The Formation Factor-Porosity Relationship: Journal of Applied Geophysics, v. 30/3, p. 215-228.

Zhang, J., 2011, Pore Pressure Prediction from Well Logs: Methods, Modifications, and New Approaches: Earth-Science Reviews, v. 108/1-2, p. 50-63.

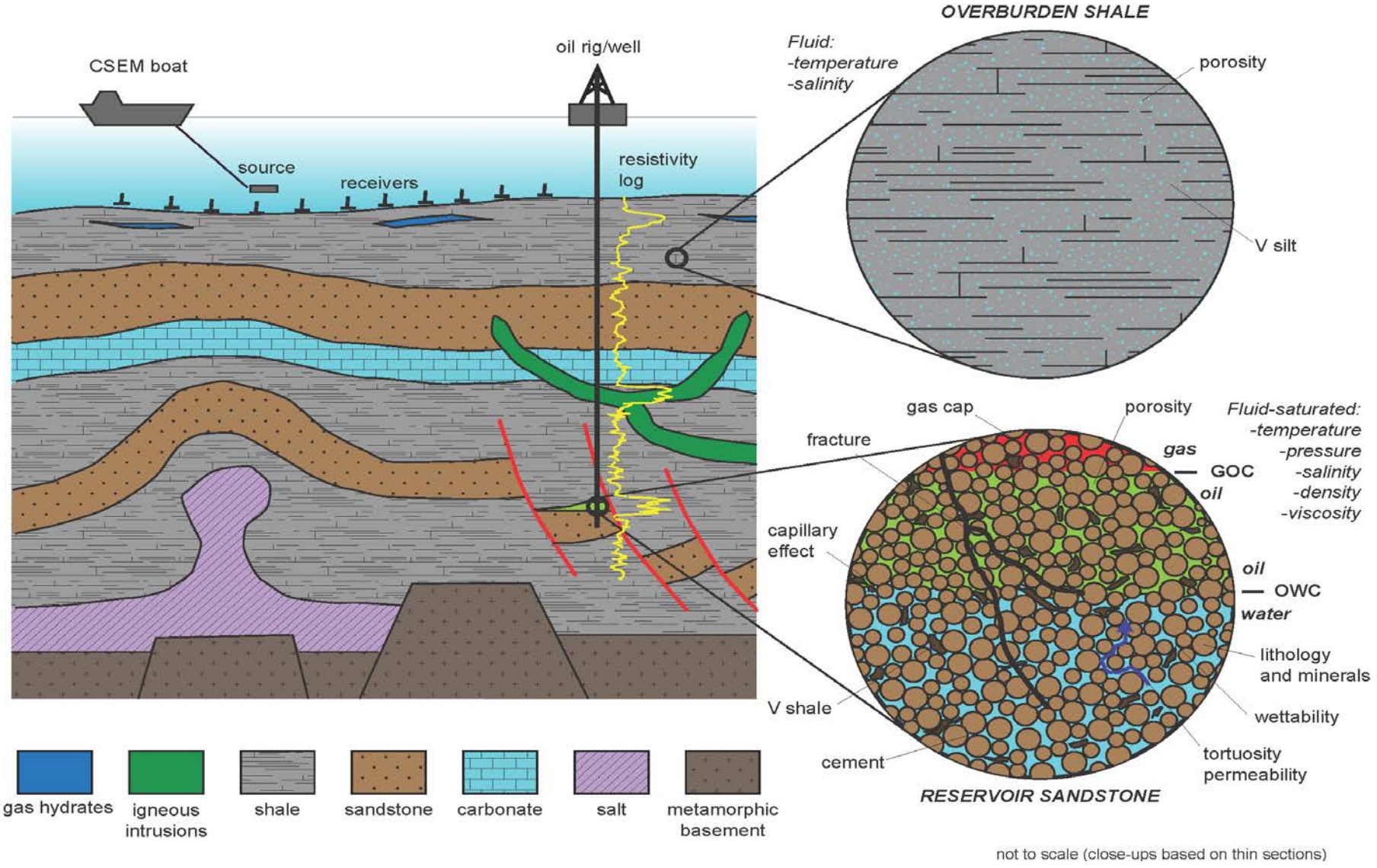

Figure 1. Schematic summary of the key parameters affecting formation resistivity in brine-bearing overburden shale and partly hydrocarbon-bearing reservoir sandstone. Non-hydrocarbon related resistive zones are also represented, as are the principal methods of measuring or deriving resistivity at a range of scales.

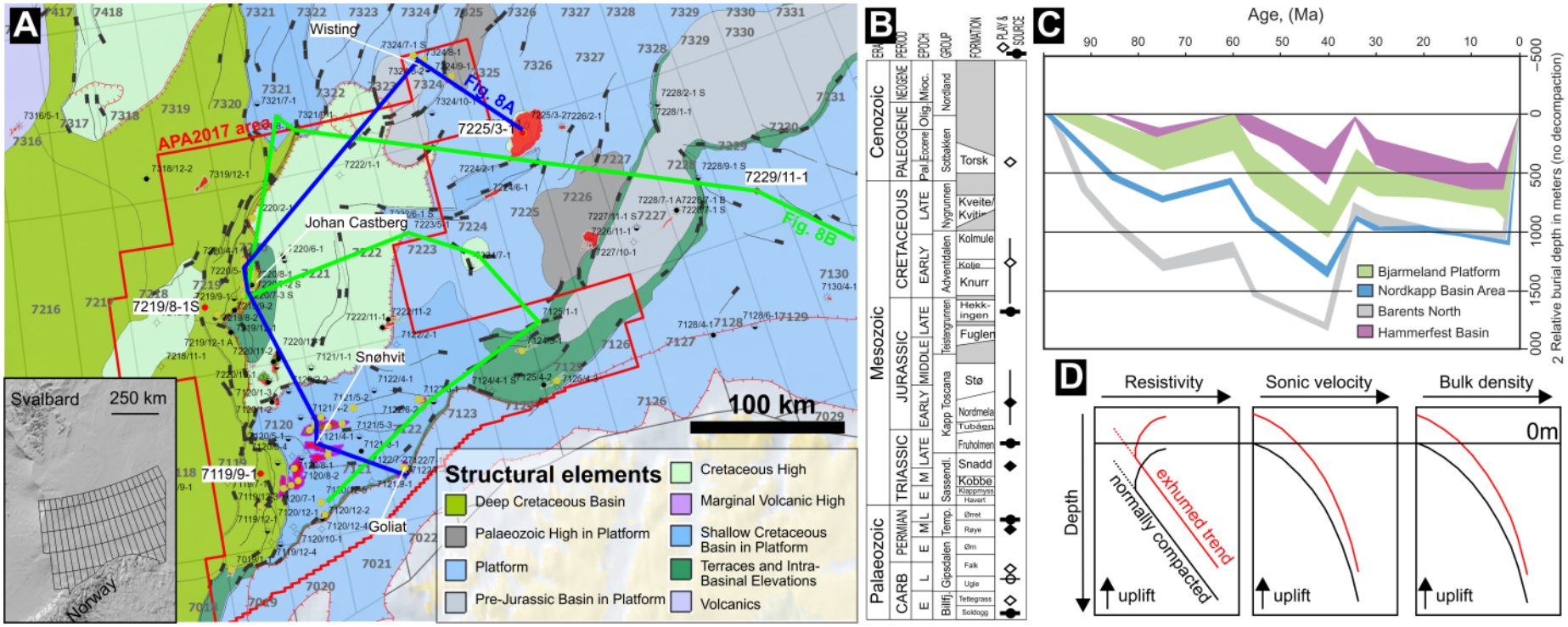

Figure 2. Tectono-stratigraphic framework of the greater Barents Sea area, illustrating the principal petroleum systems, tectonic events and sedimentary systems of the western Barents shelf. A) Structural map of the study area, courtesy of NPD (2016). Wells with hydrocarbons within the Realgrunnen Subgroup are highlighted in yellow. B) Stratigraphic column of the investigated area, based on Cavanagh et al., 2006. C) Representative subsidence curves for the last 100 Ma in different segments of the Barents shelf, reported by Ohm et al., 2008. D) Schematic representation of expected large-scale vertical trends in normally compacted (black lines) and exhumed basins (red lines). Figure inspired by Bruce and Bowers, 2002.

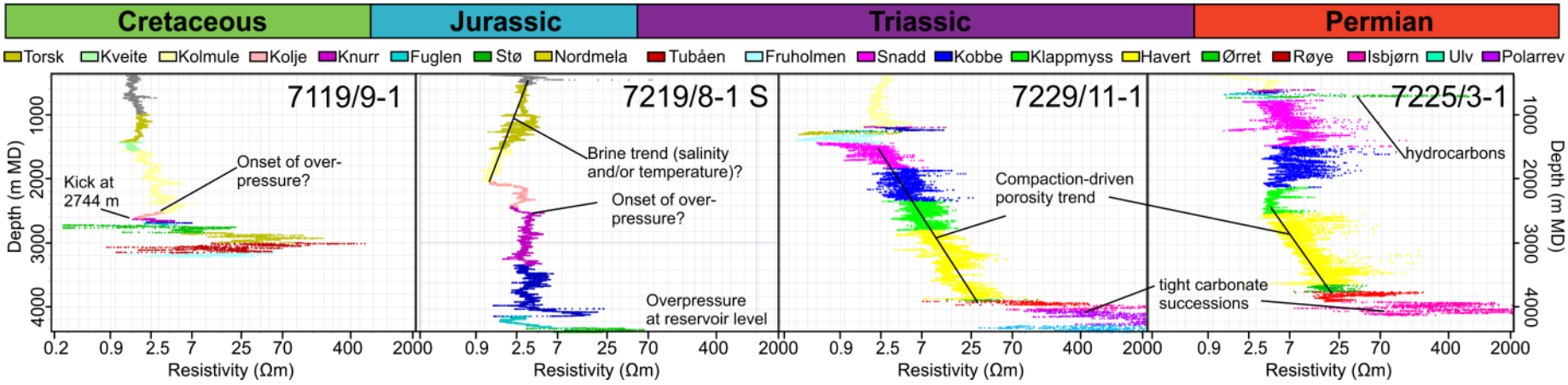

Figure 3. Variation in horizontal resistivity as a function of depth in three selected Barents Sea exploration boreholes. The boreholes were chosen to represent as much of the over- and underburden as possible. For location of the wells refer to Figure 2.

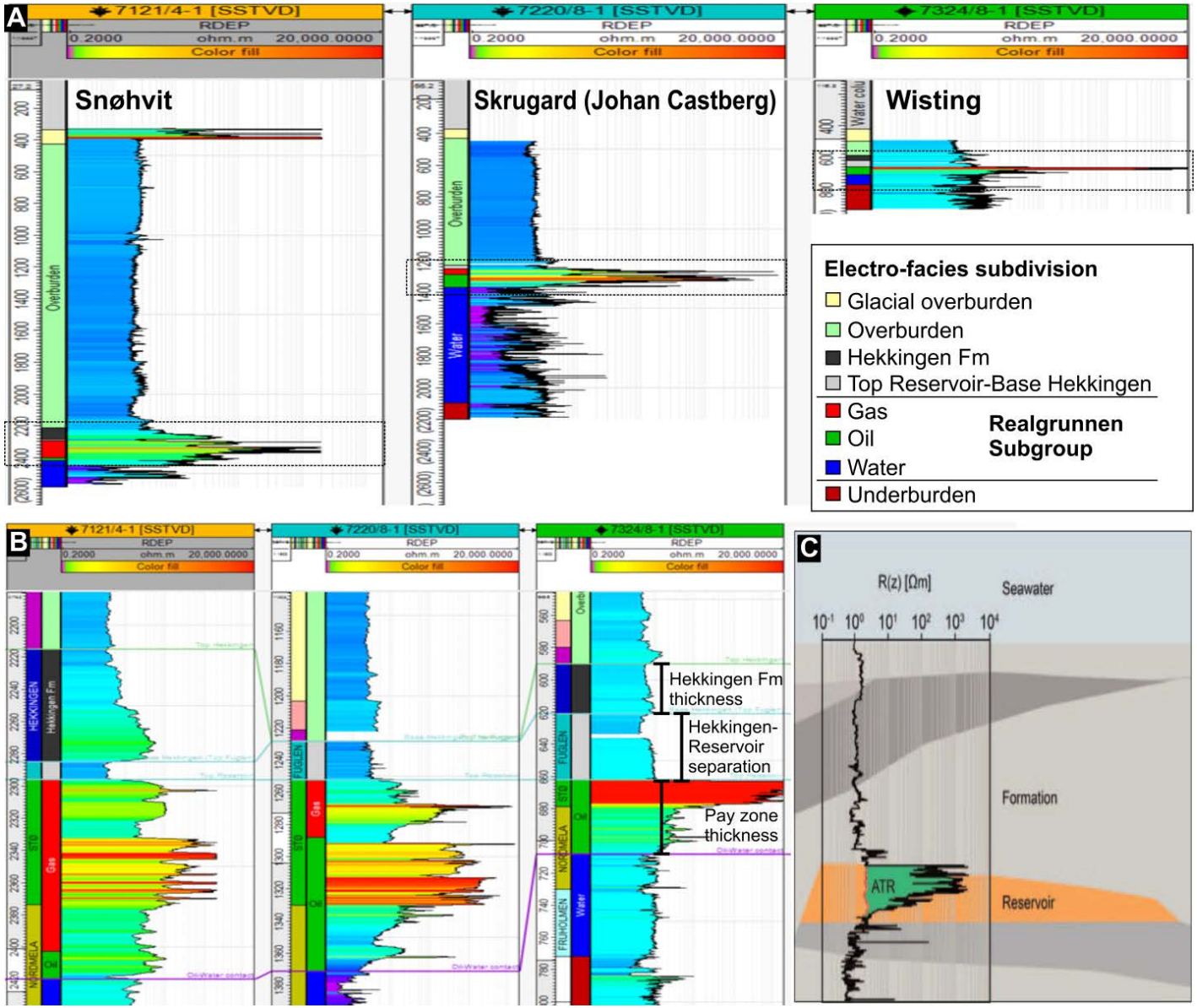

Figure 4. A) Overview of horizontal resistivity variation with depth in three selected discovery wells in the Barents Sea illustrating the subdivision applied in this study. The subdivision is fully based on the Norwegian Petroleum Directorate's FactPages and mixes formation tops and fluid contacts. B) Zoom-in of the same three wells, flattened at top reservoir level, illustrating the variation in both the Hekkingen Formation source rock interval and the Realgrunnen Subgroup reservoir. For the colour legend of the formations please refer to Figure 3. C) Schematic cartoon illustrating the concept of anomalous transverse resistance (ATR), from Baltar and Roth, 2013.

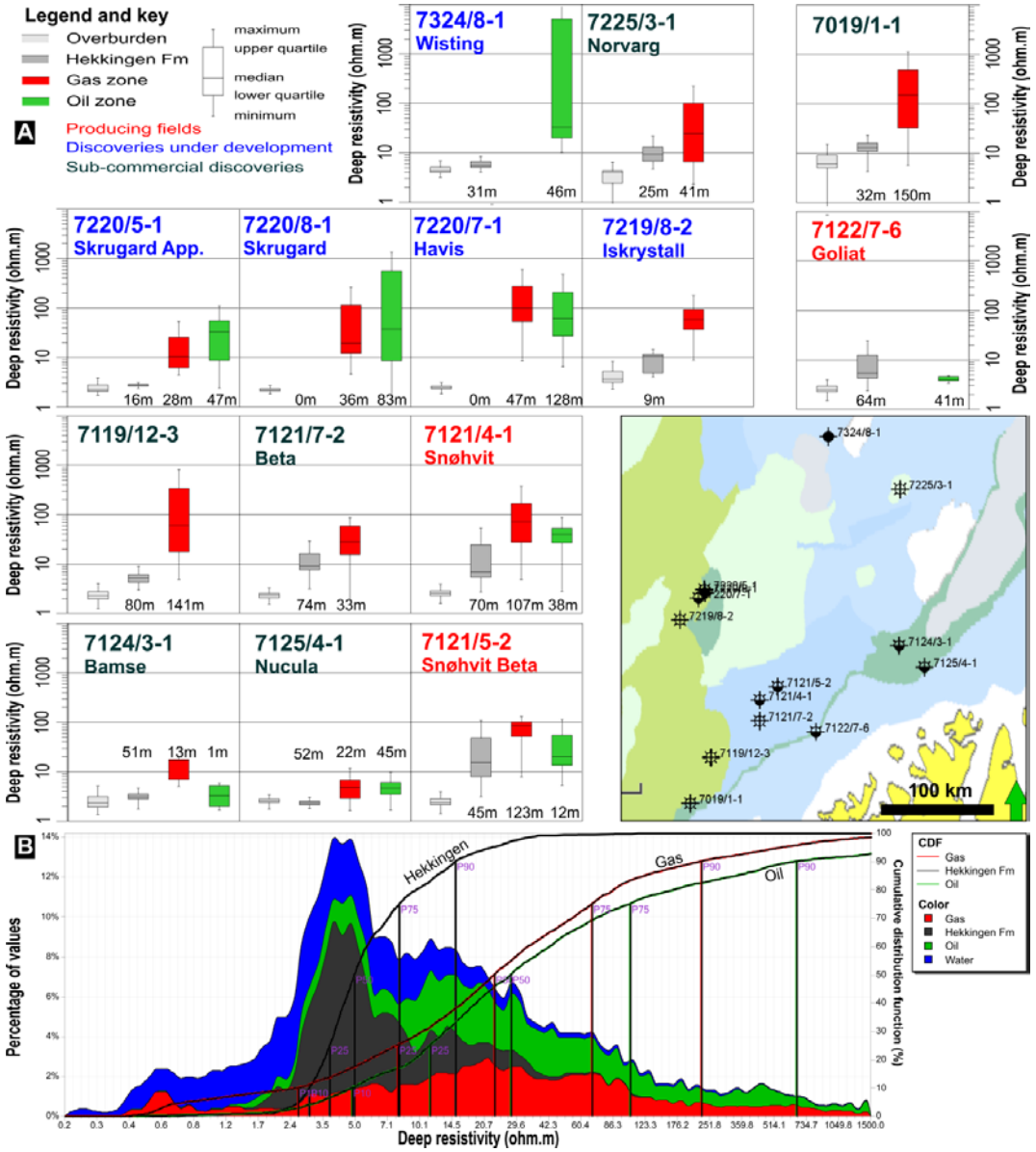

Figure 5. A) Overview of the horizontal resistivity measured in selected hydrocarbon-bearing wells in the Barents Sea, subdivided into electro-facies representing the overburden, the organic-rich Hekkingen Formation cap rock and the gas and oil zones. The inset map illustrates the wells' location, and the box-whisker plots provide a quick overview of the statistical distribution of the measured resistivity in each interval. B) Histograms illustrating the resistivity measured in the 35 hydrocarbon bearing wells, with corresponding probability functions for the Hekkingen Formation, gas and oil zones. For description of the electro-facies refer to Figure 4.

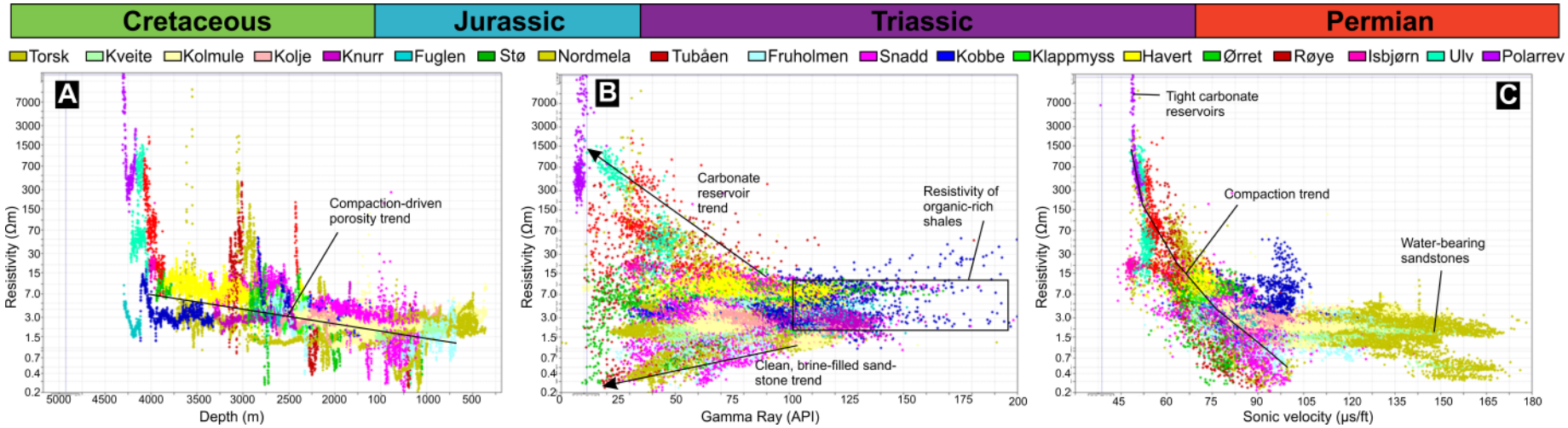

Figure 6. Cross-plots illustrating some of the parameters controlling resistivity in the non-hydrocarbon bearing overburden and underburden sections. The plots are colour-coded by formation, and different symbols signify the input well. A) Input data illustrating the depth and formation coverage of the “background” wells, and the measured resistivity, sonic velocity and gamma ray. B) Cross-plot of resistivity vs gamma ray, illustrating a clear “shale resistivity” at maximum gamma ray. C) Cross-plot of resistivity vs Sonic velocity, showing a clear correlation primarily controlled by the porosity. Non-porosity related effects (e.g., brine conductivity) overprint the main trend and result in a large spread in resistivity for a given sonic velocity.

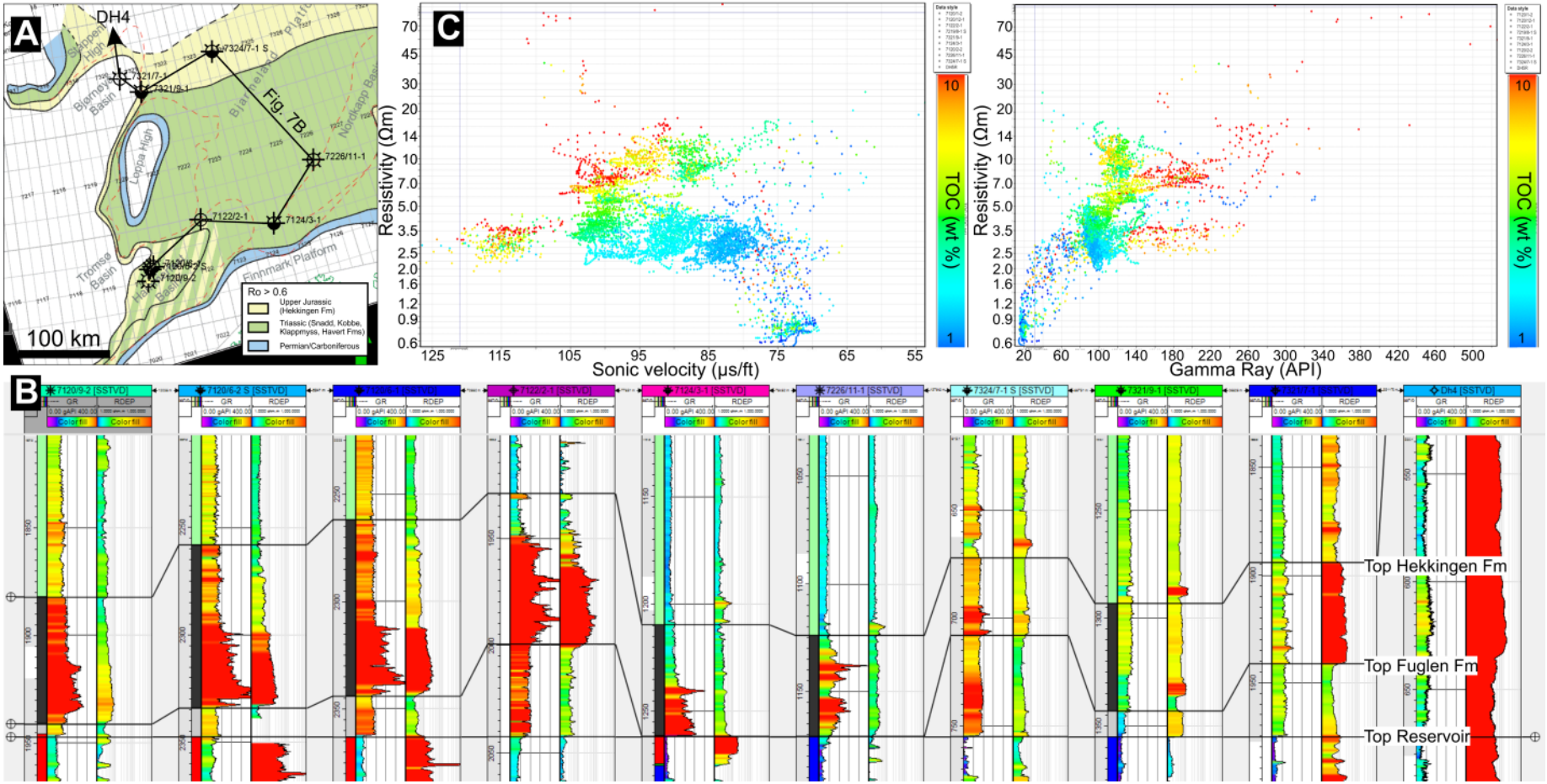

Figure 7. Resistivity variation in the organic rich shales of the Hekkingen Formation. A) Map showing wells penetrating the Hekkingen Formation, overlain by its average resistivity, thickness and the maturity map by Ohm et al., 2008. B) Well section illustrating the variation in Hekkingen Formation thickness and properties in selected exploration wells. The section is flattened on the top of the Hekkingen Formation. C) Cross-plot of resistivity vs sonic transit time, illustrating variation in TOC following the method of Passey et al., 1990.

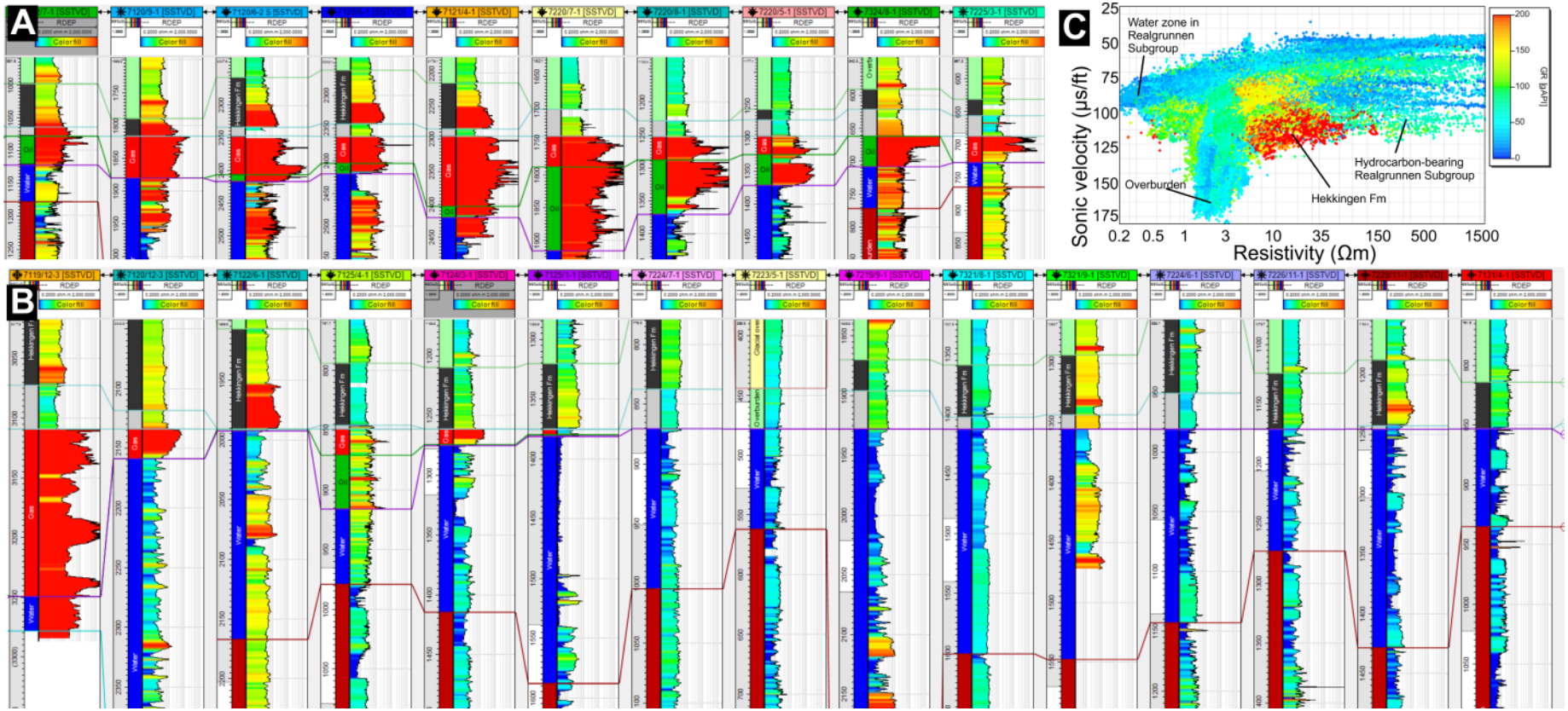

Figure 8. Overview of resistivity variation in Realgrunnen Subgroup sandstones. A) Well correlation across 10 wells from the two producing fields Goliat and Snøhvit as well as commercial discoveries Johan Castberg, Wisting, and Norvarg. B) Well correlation of wells with water-bearing or low saturation sandstones in the Realgrunnen Subgroup, including several smaller discoveries such as Arenaria and Nucula. C) Cross-plot of resistivity versus sonic velocity, colour coded by gamma ray.